Published in final edited form as:
FASEB J. 2008 February ; 22(2): 401–409.

CRMP3 is required for hippocampal *CA1* dendritic organization and plasticity

Tam T. Quach[*,1], **Guy Massicotte**[†], **Marie-Françoise Belin**[*], **Jérome Honnorat**[*], **Erica R. Glasper**[‡], **Anne C. Devries**[‡], **Lyn B. Jakeman**[§], **Michel Baudry**[¶], **Anne-Marie Duchemin**[||], and **Pappachan E. Kolattukudy**[#]

[*]*Université Lyon-1, INSERM U842, Lyon, France;* [†]*Neuroscience Research Group, Département de Chimie-Biologie, Université du Québec à Trois-Rivières, Québec, Canada;* [‡]*Departments of Psychology and Neuroscience* [§]*Department of Physiology and Cell Biology and* [||]*Department of Psychiatry The Ohio State University, Columbus, Ohio, USA;* [¶]*Neuroscience Program, University of Southern California, Los Angeles, California, USA and* [#]*Biomolecular Science Center, Burnett College of Biomedical Sciences, University of Central Florida, Orlando, Florida, USA*

Abstract

In vitro studies have pointed to the collapsin response mediator proteins (CRMPs) as key regulators of neurite outgrowth and axonal differentiation. CRMP3 is expressed mostly in the nervous system during development but remains at high levels in the hippocampus of adults. To explore CRMP3 function *in vivo*, we generated mice with targeted disruption of the CRMP3 gene. Immunohistochemistry and Golgi staining of CA1 showed abnormal dendrite and spine morphogenesis in the hippocampus of CRMP3-deficient mice. Apical dendrites displayed an increase in undulation and a reduction in length and branching points. Basal dendrites also exhibited a reduction in length with an alteration in soma stem distribution and an increased number of thick dendrites localized in stratum oriens (SO). Long-term potentiation (LTP) was impaired in this area. These data indicate an important role for CRMP3 in dendrite arborization, guide-posts navigation, and neuronal plasticity.

Keywords

Golgi analysis; gene targeting; neurite outgrowth; LTP

A growing body of evidence suggests that CRMPs play an essential role in neurite outgrowth, guidance, and axonogenesis (1). Members of this family of proteins appear to act as intracellular signaling molecules for guidance cues and neurotrophic factors. In sensory neurons, CRMP2 is required for the signal transduction cascade initiated by semaphorin 3A (Sema3A; ref. 2), a repulsive signaling molecule in axonal guidance leading to neuronal growth-cone collapse. In hippocampal neurons, it is also necessary for BDNF and NT3-induced axonal outgrowth (3). Overexpression of CRMP2 in cultured hippocampal neurons induces supernumerary axons, while a dominant-negative form suppresses the formation of the primary axon (4), confirming a role for CRMP2 in axon specification and growth. We have shown that CRMP1 is required for neurite extension induced by neurotrophin-3 (NT3) in sensory neurons (5). Overexpression of CRMP4 in cultured cortical primary neurons increases neurite length and branching (6), while overexpression of CRMP5, also known as CRAM (CRMP3-associated molecule),

[1] Correspondence: INSERM U842, Faculté de Médecine Laennec, Rue Guillaume Paradin, Lyon 69372, France, E-mail: quach.1@lyon.inserm.fr.

increases filopodia formation and supernumerary growth cones (7). CRMP3 is highly expressed during brain development, but in adults its expression is restricted to the hippocampal formation, the pontine nuclei, and the olivary complex (8). To date, little is known regarding the biological effects of CRMP3. However, we have shown that autoantibodies in sera from a subset of systemic cancer patients with limbic encephalitis react to CRMP3 (9,10). To gain further insight into CRMP3 function, we generated CRMP3-deficient (CRMP3−/−) mice by homologous recombination. Abnormalities related to the absence of CRMP3 expression indicate that CRMP3 regulates dendrite arborization and spine morphology in the hippocampus and is required for LTP formation.

MATERIALS AND METHODS

Targeting vector construct

A mouse 129/SvE genomic lambda fix library was screened with a 2.5 kb ^{32}P-labeled cDNA probe containing the entire coding region of CRMP3. The 5.0 kb *Eco*RI genomic fragment of a clone containing exons 2, 3, and 4 was subcloned into Bluescript. From this insert, the 4.7 kb *Hind*III/*Eco*RI fragment was used for the targeting construct. The unique *Cla*I site located in the middle of exon 3 was used to add a *Bam*HI site for insertion of a *Bam*HI cassette (IRES-LacZ-NeopA).

The plasmid DNA of the CRMP3 knockout construct was electroporated into R1 ES cells. Confirmation of correct targeting was established with genomic DNA isolated from individual colonies. The transmission of the target allele of a chimeric male was bred with 129/SvE females, and their progeny was genotyped. CRMP3−/− progeny, identified by PCR, was further confirmed by Western and Southern blot analysis. Briefly, genomic DNA (15 μg) was digested with *Eco*RI, separated on 1% agarose gels, and blotted on nitrocellulose filters. The ^{32}P-dCTP labeled 0.3 kb *Eco*RI-*Hind*III DNA fragment located outside the targeting vector was used as probe. For Western blots, equal amounts of proteins were separated by 10% SDS-PAGE and blots incubated with anti-CRMP3 antibody (8), followed by HRP-conjugated secondary antibody (Santa Cruz Laboratories, Santa Cruz, CA, USA) with Enhanced Chemiluminescence (Amersham Biosciences, Piscataway, NJ, USA) detection. Primers derived from the LacZ sequence [LacZS (AGCAGAAGCCGTCGATGTCG)/LacZA (ACCGTTCATACA GAACTGG)] and from the intronic regions surrounding exon 3 [P3 (GGCAGATAGGTAACCAT-TTGG)/P4(GCATTTACAGAAACCCAGCC)] were used to identify CRMP3−/− progeny by PCR.

Histology

Male animals (3 months old) were used for histology and electrophysiology experiments. Normal and mutant littermate mice brains were processed in parallel, and all data were analyzed by an investigator blind to the genotype. Standard immunohistochemistry, β-galactosidase, and Golgi staining were performed to analyze cell morphometry. For β-galactosidase staining, serially cut 30-μm-thick cryosections of fixed brains were incubated with X-gal solution (5 mM potassium ferricyanide, 5 mM potassium ferrocyanide, 2 mM $MgCl_2$, and 1 mg/ml 5-bromo-4-chloro-3-indoyl-β-D-galactopyranoside in PBS) at 37°C for 10–12 h. For immunohistochemistry, 10–20 μm cryostat sections were collected on Superfrost Plus slides, permeabilized with 0.1% Triton X-100 in PBS containing 1% gelatin, and stained with the following antibodies: mouse monoclonal against MAP2 (1/2500 dilution, Chemicon International, Temecula, CA, USA) and rabbit polyclonal against MAP2 (1/2000, Sigma, St. Louis, MO, USA) and β-galactosidase (1/1000, Promega, Madison, WI, USA). Sections were incubated with one or more of the secondary antibodies (Alexa Fluor 546-coupled anti-rabbit IgG and Alexa Fluor 488-coupled anti-mouse IgG; 1/2000, Molecular Probes, Eugene, OR, USA). Some sections were incubated with a 0.1 μg/ml solution of DAPI (4,6-diamidino-2-

phenylindoldihydrochloride, Sigma) to label cell nuclei. Sections were viewed using an epifluorescent Zeiss microscope. Golgi staining was performed according to the manufacturer's instructions (Rapid Golgi Staining Kit, FD Neurotechnologies, Inc., Ellicott City, MD, USA). Coronal sections (150 μm) containing identical regions of the hippocampal formation were selected from wild-type (WT) and CRMP3−/− mice for analysis. Neurons chosen for camera lucida tracing were impregnated entirely with Golgi stain and were not obscured by other neurons. All neurites were visible within the plane of focus. For quantification of the undulation of apical dendrites, a linearity index was calculated by computer-assisted measurement of apical dendrite lengths (100 μm from the cell body) using MCID *Elite* image analysis software (Imaging Research, Inc., St. Catherine's, ON, Canada). The linearity index is defined as the curvilinear length in micrometers of a region of the apical dendrite divided by the linear distance between the ends of the region measured (11). Spines were assigned the morphology category that most resembled the shape of that spine. The length of each spine was defined as the distance from the distal surface of the spine head to the dendrite in micrometers. Finally, spines were counted at 50-μm-long distance from the soma in the stratum oriens. To avoid potential interference of thick apical dendritic diameter on spine morphometry in stratum radiatum, we analyzed spines density and length on oblique dendritic arbors of apical dendrites. Spine density was defined as number of spines per 25 μm of dendrite. Statistical significance was assessed by paired two-tailed *t* test, with significance set at $P < 0.05$.

Hippocampal slice electrophysiology

LTP was elicited by applying theta burst stimulation (TBS) (10 bursts of 4 stimulation pulses at 100 Hz delivered at 200-μs intervals). Parameters of evoked fEPSPs were normalized to the values of their respective means measured during the baseline-recording period. Hippocampal slices were prepared as described previously by Kramar *et al.* (12). Briefly, brains from male WT and CRMP3−/− mice (n=7) were placed in oxygenated dissection medium containing 124 mM NaCl, 3 mM KCl, 1.25 mM KH_2PO_4, 5 mM $MgSO_4$, 3.4 mM $CaCl_2$, 26 mM $NaHCO_3$, and 10 mM glucose. Field excitatory postsynaptic potentials (fEPSP) were recorded from stratum radiatum of CA1b using a single pipette filled with 0.15 M NaCl (with a resistance of 2–3 MΩ) in response to orthodromic stimulation (twisted nichrome wires, 65 μm) of the Schaffer collateral-commissural projections in CA1 stratum radiatum. Pulses were delivered to the stimulation electrode at 0.033 Hz with current test intensity adjusted to obtain 50–60% of the maximal fEPSP. Recorded evoked potentials were digitized and several parameters (fEPSP slope, amplitude, and area) analyzed using pCLAMP 9.0 (Axon Instruments/Molecular Devices, Sunnyvale, CA, USA). LTP was elicited by applying theta burst stimulation (TBS) (10 bursts of 4 stimulation pulses at 100 Hz delivered at 200-μs intervals). Parameters of evoked fEPSPs were normalized to the values of their respective means measured during the baseline-recording period. Values given in the text are means ± SEM, and statistical significance was assessed by paired Student's Wilcoxon *t* tests, with significance set at $P < 0.05$. Representative traces are averages of 10 sweeps.

RESULTS

Targeting inactivation of the CRMP3 gene and general appearance of CRMP3−/− mice

A targeting vector was designed to disrupt the CRMP3 gene at exon 3. The mutation consisted of insertion of stop codons in all three reading frames with an IRES linked to a LacZ open reading frame with SV40 polyadenylation site, extended with a neomycin resistance gene that was expressed independently with its own promoter (Fig. 1A). The LacZ-Neomycin cassette insertion disrupts the CRMP3 gene and makes it possible to identify CRMP3-expressing cells by visualizing β-galactosidase. The homozygote genotype was confirmed by a change in size of *Eco*RI-DNA genomic fragment revealed by Southern blot (Fig. 1*B*) or PCR (Fig. 1*C*).

Western blot analysis with an anti-CRMP3 antibody directed against the peptide MVPAKPGSGAPARASC showed the loss of CRMP3 gene product (Fig. 1*D*). Thus, we conclude that this targeted LacZ-Neo insertion resulted in a null mutation of the CRMP3 gene.

CRMP3−/− mice grew normally and did not present major organ defect. In particular, no gross abnormality was seen in hippocampus, cerebellum, neocortex, thalamus, and striatum of CRMP3−/− or CRMP3+/−mice by light microscopy of cresyl violet- or DAPI-stained sections (not shown). β-Galactosidase activity staining to map CRMP3 gene expression confirmed previous results (8,13). An intense blue color was seen and remained unchanged in 1-wk- to 6-month-old animals in the pontine nuclei, olivary complex and the hippocampus (Fig. 1*E*). Within the hippocampus, LacZ activity was strong in stratum pyramidal (SP) and stratum radiatum (SR) of field CA1 (Fig. 1*F*), CA3, and dentate gyrus. Blue coloration was also seen in several nuclei of the thalamus and in the dorsal part of the reticular formation. LacZ expression in cerebellum decreased with age starting at postnatal day 14, with only few cells in the granular layer displaying blue coloration in 4- to 5-wk-old mice. To investigate possible correlations between structural and functional abnormalities, we analyzed the morphological and electro-physiological characteristics of the CA1 pyramidal neurons of CRMP3−/− mice.

Abnormal neurite outgrowth and lamination in the hippocampus of CRMP3−/− mice

In WT mice, examination with MAP2 and Golgi staining revealed obvious laminar cytoarchitectoral organization with neuronal perikarya disposed in a single compact lamina. The single primary apical dendrite emerged from the neuronal cell body, branched within stratum radiatum in a well-developed arbor, running relatively straight and projecting for long distance in the plane of the section (Fig. 2*A*), suggesting that these dendrites need guidance for proper orientation and positioning within the brain. In contrast, in CRMP3−/− mice, the MAP2-positive apical dendrites were poorly aligned and wavier in appearance (Fig. 2*B*). These findings were confirmed with Golgi impregnation (Fig. 2*C*, *D*). In CRMP3−/− mice, a significant number of pyramidal neurons display tortuous/undulating apical dendrites (CRMP3 −/−, 42%; WT, 6%; Fig. 2*H*) that were morphologically distinct (Fig. 2*D–E*) from the straight apical dendrites of WT mice (Fig. 2*C*). The mean linearity index for apical dendrites of pyramidal neurons from WT mice was 1.06 ± 0.01, whereas that of apical dendrites from CRMP3−/− mice was 1.30 ± 0.05 (Fig. 2*I*). Interestingly, hippocampal pyramidal axons that run through the alveus (Fig. 2*F–G*) and dendrites from cortical pyramidal neurons from CRMP3−/− mice were not undulated (Fig. 3). In addition, the number of branching on primary (PD) and secondary (SD) apical dendrites of CA1 pyramidal cells from CRMP3−/− mice was decreased (PD: WT, 16.2±0.2, CRMP3−/−, 12.3±0.1, $P<0.05$; SD: WT, 12.0±0.7, CRMP3−/ −, 6.1±0.5, $P<0.01$) with a reduced total dendritic length (WT, 1920±71 μm, CRMP3−/−, 1242 ±47 μm, $P<0.01$; Fig. 2*J*, *K*).

The distribution pattern of basal somata stems (BSS) per cell was also different between the two genotypes (Fig. 2*L*; see Supplemental Fig. 1, left). In WT, 50% of pyramidal cells displayed 4 BSS, each bearing 10 –12 basal primary dendrites (BPD). A significant decrease was found in the number of cells bearing 4 BSS (Fig. 2*L*) and in BPD per cell in CRMP3−/− mice (WT, 10.85±0.47, CRMP3−/−, 6.75±0.60, $P<0.01$) while the number of BPD/BSS was not different (WT, 2.75±0.38, CRMP3−/−, 2.60±0.20), suggesting that the decrease in BPD was related to the impairment in BSS. A reduction in total basilar dendritic length was also observed in CRMP3−/− mice (WT, 1387±99 μm, CRMP3−/−, 1005±38 μm, $P<0.05$).

Finally, staining with two antibodies against MAP2 showed an outgrowth of thick dendrites (>2.5 μm) that extended into and throughout SO in CRMP3−/− mice (Fig. 4*B*) and resulted in a significant increase in the density of neurites (1.4±0.1 and 56.5±6.3 neurites/0.01 mm^2 for WT and CRMP3−/−, respectively; $P<0.0001$). Many of these thick dendrites originated from the pyramidal cell layer (Fig. 4*C*), suggesting a likely—and at least partially—pyramidal

origin. These observations are consistent with data obtained from Golgi preparations, which revealed a significant increase in the number of cells bearing thick neurites projecting to SO (1.7±0.5 and 5.0±0.6 cells/field for WT and CRMP3−/−, respectively; Fig. 4*F*). Interestingly, in CRMP3−/− mice, some cells lacked a typical thick apical dendrite projecting in SR and instead displayed a cluster of thin, short neurites (Fig. 4*E*) or several misoriented apical dendrites running parallel to the SP layer (see Supplemental Fig. 1, right). These characteristics were never observed in WT mice.

Dendritic spine alterations in pyramidal neurons of CRMP3−/− mice

Several subtypes of spines—stubby, finger, cup, and mushroom—are found by Golgi-staining of pyramidal cells in hippocampal CA1 of adult CRMP3−/− mice (Fig. 5*C–E*), suggesting that CRMP3 is not associated with the development of a particular spine shape *per se*. In addition, no significant difference was found in spine density (Fig. 5*A, B*) for a given distance along the secondary apical (WT: 27±2.0 spines/25 μm; CRMP3−/− : 26±2.0 spines/25 μm, $P<0.05$) or basal dendrites (WT: 26±3.0 spines/25 ±m; CRMP3−/− : 25±2.0 spines/25 μm, $P<0.05$) of CA1 pyramidal cells between genotypes, although a trend shows a slight decrease in mushroom spines and a slight increase in finger spines (see Supplemental Information, T.1 and T.2). In contrast, significant differences in mushroom and finger length were found between genotypes in both SO and SR. These two spine types were significantly shorter in CRMP3−/− than in WT mice ($P<0.004$; Fig. 5*F*). Thus, the processes leading to formation of novel spines might be CRMP3-independent, while the processes leading to elongation of spines are at least partially CRMP3-dependent. Dendritic spines are sites of biochemical compartmentalization and sources of electrical activities, and their function seems to be associated with their shape and size. It has been found that the decay of intrasynaptic Ca^{23} depends on the length of the spines (14). The altered size of CRMP3−/− spines is likely to generate a different electrophysiological pattern that may influence various functional changes in CRMP3−/− hippocampus.

Impairment of LTP induction in CA1 of CRMP3−/− mice

The abnormalities in pyramidal cell morphology and spines are of particular interest since these cells are key components in the trisynaptic circuit, thought to play a major role in LTP. In consequence, we performed electrophysiological experiments in hippocampal slices to investigate a potential physiological correlation to the CA1 pyramidal dendrite abnormalities. No alterations in basal synaptic transmission (Fig. 6*A*) or paired pulse facilitation (Fig. 6*B*) were found. However, the analysis of fEPSP during TBS indicates that physiological events required for LTP induction were disrupted in CRMP3−/− mice. As shown in Fig. 6*C*, CRMP3 −/− exhibited a significant decrease in the magnitude of LTP in hippocampal slices prepared from area CA1 of CRMP3−/− mice (23±8%) when compared to controls (60±6%; $P<0.05$; *t* test). The fEPSP slope at 1 min was similar for both groups (72±7% for CRMP3−/−, 81±7% for WT). Previous work has shown that, relative to the initial burst, subsequent burst responses during TBS exhibit an important component mediated by activation of NMDA receptors. As illustrated in Fig. 6*D*, slices prepared from CRMP3−/− mice exhibited a significant reduction in burst response numbers 2, 4, and 6, which reached, respectively, 86 ± 10%, 108 ± 11%, and 116 ± 16% increases in WT mice but only 42 ± 5%, 51 ± 6%, and 43 ± 7% in CRMP3−/− mice. These results demonstrate a deficit in LTP formation and strongly suggest abnormalities in neural plasticity in the CRMP3−/− mice.

DISCUSSION

During development, neurite outgrowth and specific connections between neurons and their targets are determined, at least in part, by guidance molecules. When the intracellular signaling pathways for these molecules are selectively disturbed, structural impairments, inappropriate laminar organization, and hippocampal dysfunction can occur. CRMPs, which are particularly

abundant in hippocampus, are implicated in the semaphorin signal transduction pathway, inducing growth cone collapse, and in the neurite extension controlled by neurotrophins. Therefore, they may participate in the regulation of neurite outgrowth and wiring of this structure. Indeed, the present analysis of mice with disruption of the CRMP3 gene supports a role for CRMP3 in dendrite organization in hippocampus. CRMP3−/− mice display a significant decrease in dendritic length and branching points and an abnormal undulation of apical primary dendrites. This abnormal undulation is likely due to the altered signaling of CRMP3-dependent guideposts proteins directing point to point navigation of growth cone on the spatial array (15). Interestingly, a similar pattern has been described in L1 knockout mice (11). L1 is the coreceptor of the Neuropilin 1 receptor complex for Sema 3A. To a lesser degree, dendrite misorientation is also present in Sema3A- and Fyn-deficient mice (16). CRMP4 (6) and cypin (17), which shares strong homology with the CRMP family, have also been shown to have a role in dendrite branching.

Another intriguing observation obtained from immunohistochemistry in CRMP3−/− mice was the higher incidence of thick MAP2-positive dendrites projecting to SO (Fig. 4). MAP2 is essential for establishing proper dendritic extension. It stabilizes microtubules and modifies cytoskeletal dynamics (18). The absence of CRMP3 may lead to a molecular cascade dissociation that might eventually influence the normal accumulation and function of MAP2. Golgi staining also revealed an increase in cells bearing these atypical dendrites. Since only a small portion of neurons are stained with Golgi impregnation, it was not possible to quantitatively and directly compare data obtained with the two techniques. Nonetheless, these combined findings suggest that CRMP3 is a critical factor participating in the signaling mechanism of dendrite growth and orientation in hippocampus. Ectopic and hypertrophic dendrites and axons were also found in hippocampus of mice with selective Pten deletion (19). In contrast to the effects of Pten deletion, however, no axonal abnormalities were detected in CRMP3−/− mice by Tau (not shown) or Golgi (Fig. 2*F–G*) staining, suggesting that CRMP3 regulates only the arborization and patterning of dendrites in this brain region. Furthermore, the absence of abnormal undulations of pyramidal dendrites in the cerebral cortex of the same animals, where CRMP3 is not expressed, confirms the specific role of CRMP3 in hippocampus.

The molecular mechanisms underlying the hippocampal dendritic abnormalities are unknown although it has been recently shown that other CRMPs promote microtubule dimerization (20) and F-actin bundling *in vitro* (21). Similarly, CRMP3 may mediate dendritic patterning and spine outgrowth through rearrangement of the cytoskeleton. Remodeling of dendritic arbors and spines is considered to represent the structural support of synaptic plasticity. In adult CRMP3-deficient mice, abnormal dendritic organization and spine morphology of CA1 were not associated with major differences in AMPA receptor-mediated synaptic transmission and paired-pulse facilitation, which suggests that the basic features of synaptic transmission were not markedly impaired. CRMP3 deficiency did cause, however, a marked reduction in LTP in this brain structure (Fig. 6). Previous investigations have shown that inhibitory postsynaptic potentials (IPSPs), which normally truncate EPSPs, are prominent during the first burst of the TBS train but are largely absent in subsequent bursts. As a result, these subsequent bursts exhibit buildup of depolarization due to a transient reduction of IPSPs and activation of NMDA receptors. The spatial pattern of dendritic organization plays an important role in neuronal function. Dendrites and spines are critical in particular for LTP formation. Abnormalities in their morphology may thereby impede the correct formation of synaptic contact and connections, and could be responsible for the LTP deficit observed in CRMP3−/− mice. Notably, TBS induces actin polymerization in dendritic spines during LTP (22), which could be impaired in CRMP3−/− mice. Conceivably, CRMP3 may also be a direct component of the complex glutamate intracellular signaling pathway involved in LTP induction and maintenance. Consistent with this hypothesis, cypin has been implicated in the postsynaptic trafficking of PSD-95, the NMDA receptor-anchoring protein (23) and a CRMP2 isoform

regulates the surface expression of NMDA receptor subunits (24). Interestingly, an alteration in MAP2 staining and a deficit in LTP were also detected in hippocampus of CRMP1−/− mice (25).

Marked alterations in neuronal morphology are found in CRMP3−/− mouse brain. Interestingly, alterations in spine morphology, dendritic arborization, and abnormal neuronal orientation are found in Down syndrome brain where the expression of CRMP3 gene is also impaired (26).

Acknowledgements

We thank Dr. Bedrich Mosinger and the Keck Facilities (Ohio State University) for their help in the generation of the mouse line and Dr. Marcel Tappaz for analyzing immunohistochemical data blind to the genotype of the animals. This research was supported by INSERM and Region Rhone Alpes, AFM.

References

1. Charrier E, Reibel S, Rogemond V, Aguera M, Thomasset N, Honnorat J. Collapsin response mediator proteins (CRMPs): Involvement in the nervous system development and adult neurodegenerative disorders. Mol Neurobiol 2003;28:51–64. [PubMed: 14514985]
2. Goshima Y, Nakamura F, Strimatter P, Strimatter SM. Collapsin-induced growth cone collapse mediated by an intracellular protein related to unc-33. Nature 1995;376:509–514. [PubMed: 7637782]
3. Yoshimura T, Kawano Y, Arimura N, Kawabata S, Kikuchi A, Kaibuchi K. GSK-3 beta regulates phosphorylation of CRMP-2 and neuronal polarity. Cell 2005;120:137–149. [PubMed: 15652488]
4. Inagaki N, Chihara K, Arimura N, Ménager C, Kawono Y, Matsuo N, Nishimura T, Amano M, Kaibuchi K. CRMP2 induces axons in cultures hippocampal neurons. Nat Neurosci 2001;4:781–782. [PubMed: 11477421]
5. Quach TT, Duchemin AM, Rogemond V, Aguera M, Honnorat J, Belin MF, Kolattukudy P. Involvement of collapsin response mediator proteins in the neurite extension produced by neurotrophins in dorsal root ganglions neurons. Mol Cell Neurosci 2004;25:433–443. [PubMed: 15033171]
6. Quinn CC, Chen E, Kinjo T, Kelly G, Bell AW, Elliott RC, McPherson PS, Hockfield S. TUC-4b, a novel TUC family variant, regulates neurite outgrowth and associated with vesicles in the growth cone. J Neurosci 2003;23:2815–2823. [PubMed: 12684468]
7. Hotta A, Inatome R, Yuasa-Kawada J, Quin Q, Yamamura H, Yanagi S. Critical role of collapsin response mediator protein-associated molecule CRAM in filopodia and growth cone development in neurons. Mol Biol Cell 2005;16:32–39. [PubMed: 15509652]
8. Quach TT, Mosinger B Jr, Ricard D, Copeland NG, Gilbert DJ, Jenkins NA, Stankoff S, Honnorat J, Belin MF, Kolattukudy P. CRMP3/unc33-like protein 4 gene: organization, chromosomal mapping and expression in the developing mouse brain. Gene 2000;242:175–182. [PubMed: 10721710]
9. Honnorat J, Byk T, Kushers I, Aguera M, Ricard D, Rogemond V, Quach T, Aunis D, Sobel A, Mattei MG, Kolattukudy P, Belin MF, Antoine JC. Ulip/CRMP proteins are recognized by autoantibodies in paraneoplastic neurological syndromes. Eur J Neurosci 1999;11:4226–4232. [PubMed: 10594648]
10. Knudsen A, Bredholt G, Stortein A, Honnorat J, Vedeler CA. Antibodies to CRMP3–4 associated with limbic encephalitis and thymoma. Clin Exp Immunology 2007;49:16–22.
11. Demyanenko GK, Tsai AY, Maness PF. Abnormalities in neuronal process extension, hippocampal development, and the ventricular system of L1 knockout mice. J Neurosci 1999;19:4907–4920. [PubMed: 10366625]
12. Kramar EA, Lin B, Lin CY, Arai AC, Gall CM, Lynch G. A novel mechanism for the facilitation of theta-induced long term potentiation by brain-derived neurotrophic factor. J Neurosci 2004;24:5151–5161. [PubMed: 15175384]
13. Wang LH, Strittmatter SM. A family of rat CRMP genes is differentially expressed in the nervous system. J Neurosci 1996;16:6197–6207. [PubMed: 8815901]
14. Segal M, Korkotian E, Murphy D. Dendritic spine formation and pruning: common cellular mechanisms? Trends Neurosci 2000;23:53–57. [PubMed: 10652540]

15. O'Connor TP, Bentley JS. Accumulation of actin in subsets of pioneer growth cone filopodia in response to neural and epithelial guidance cues in situ. J Cell Biol 1990;123:935–948.
16. Sasaki Y, Cheng C, Uchida Y, Nakajima O, Oshshima T, Yagi T, Taniguchi M, Nakayama T, Kishida R, Kudo Y, Ohno S, Nakamura F, Goshima Y. Fyn and Cdk5 mediate Semaphorin-3A signaling, which is involved in regulation of dendrite orientation in cerebral cortex. Neuron 2000;35:907–920. [PubMed: 12372285]
17. Akum BF, Chen M, Gunderson SI, Riefler GM, Scerri-Hansen MM, Firestein BL. Cypin regulates dendrite patterning in hippocampal neurons by promoting microtubule assembly. Nat Neurosci 2004;7:145–152. [PubMed: 14730308]
18. Ozer RS, Halpain S. Phosphorylation-dependent localization of microtubule-associated protein MAP2c to the actin cytoskeleton. Mol Biol Cell 2000;11:3573–3587. [PubMed: 11029056]
19. Kwon CH, Luikart BW, Powell CM, Zhou J, Baker SJ, Parada LF. Pten regulates neuronal arborization and social interaction in mice. Neuron 2006;50:377–388. [PubMed: 16675393]
20. Fukata Y, Itoh TJ, Kimura T, Ménager C, Nishimura T, Shiromizu T, Watanabe H, Inagaki N, Iwamatsu A, Hotani H, Kaibuchi K. CRMP2 binds to tubulin heterodimers to promote microtubule assembly. Nat Cell Biol 2002;4:583–591. [PubMed: 12134159]
21. Rosslenbroich V, Dai L, Baader SL, Noegel AA, Gieselmann V, Kappler J. Collapsin response mediator protein-4 regulates F-actin bunddling. Exp Cell Res 2005;310:434–444. [PubMed: 16181627]
22. Lin B, Kramar EA, Bi X, Brucher FA, Gall CM, Lynch G. Theta stimulation polymerizes actin in dendritic spines of hippocampus. J Neurosci 2005;25:2062–2069. [PubMed: 15728846]
23. Firestein BL, Brenman JE, Aoki C, Sanchez-Perez AM, El Husseini AE, Bredt DS. Cypin: a cytosolic regulator of PSD-95 post-synaptic targeting. Neuron 1999;24:659–672. [PubMed: 10595517]
24. Bretin S, Rogemond V, Marin P, Maus M, Torrens Y, Honnorat J, Glowinski J, Prémont J, Gauchy C. Calpain product of WT-CRMP2 reduces the amount of surface NR2B NMDA receptor subunit. J Neuroschem 2006;98:1252–1265.
25. Su KY, Chien WL, Fu IS, Huang HP, Lin SR, Shih JY, Lin YL, Hsueh YP, Yang PC, Lin SW. Mice deficient in CRMP1 exhibit impaired long-term potentiation and impaired spatial learning and memory. J Neurosci 2007;27:2513–2524. [PubMed: 17344389]
26. Weitzdoerfer R, Fountoulakis M, Lubec G. Aberrant expression of dihydropyraminidase related proteins-2,-3 and -4 in fetal Down syndrome brain. J Neural Transm Suppl 2001;61:95–107. [PubMed: 11771764]

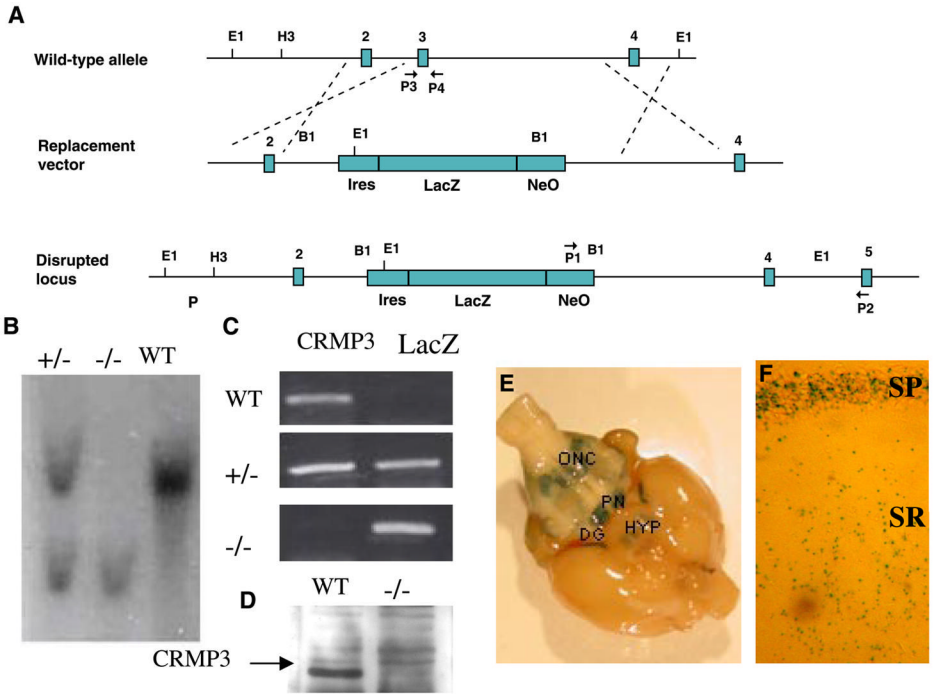

Figure 1.

Characterization of CRMP3−/− mice. *A)* The WT allele, the targeting vector, and the targeted allele expected following homologous recombination (numbered boxes indicate exons; letters with arrows indicate the primers used for PCR analyses). B1, BamH1; E1, *Eco*RI, H3, *Hind*III; P, Probe. *B)* Southern blot analysis of genomic DNA isolated from liver of WT, CRMP3+/−, and CRMP3−/− mice. The disrupted allele contains a new *Eco*RI restriction site, generating a 2.4 kb fragment. *C)* Mice were genotyped with 2 PCR primer sets (P3/P4; NeoS/NeoA). *D)* Western blot analysis. Total protein (20 μg) from hippocampus of WT and CRMP3 −/− mice incubated with specific anti-CRMP3 antibodies shows 66 kDa CRMP3 protein in the WT and no protein in the mutant. *E)* Whole mount showing lacZ activity driven by CRMP3 gene promoter in CRMP3−/− adult brain. *F)* LacZ staining of CA1 region.

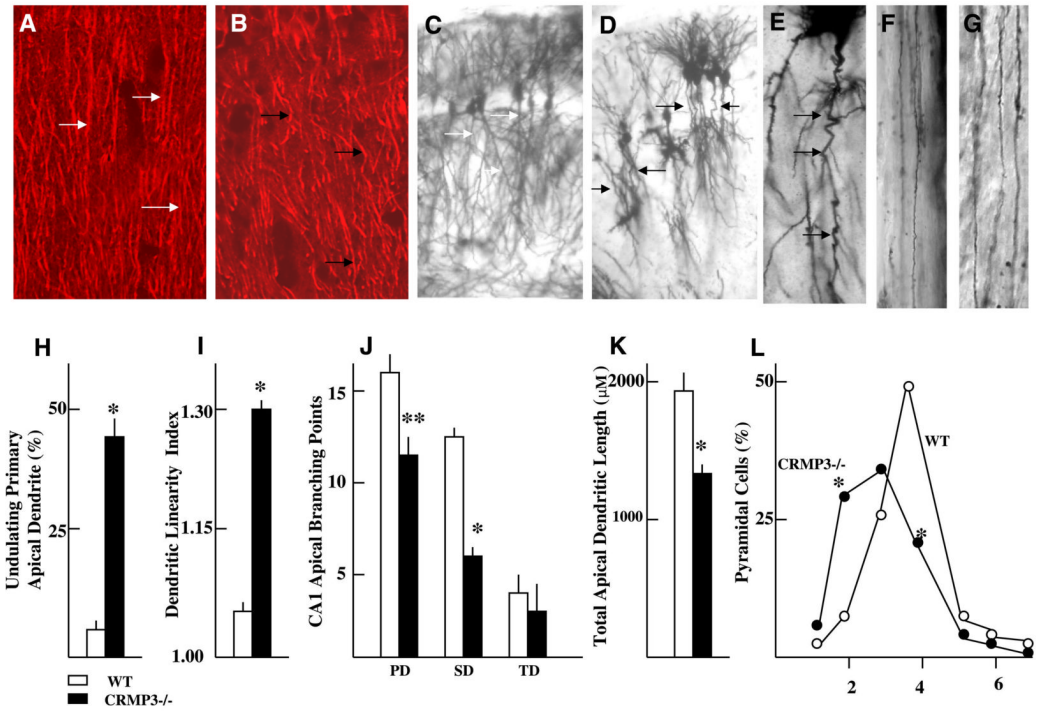

Figure 2.

Abnormal dendritic pattern in CA1 of CRMP3−/− mice. Qualitative analysis of pyramidal neurons: *A, B*) MAP2-staining with monoclonal antibody of coronal sections of hippocampus from 3-month-old WT (*A*) and CRMP3−/− (*B*) mice. *C, D)* Golgi staining of hippocampus from WT (*C*) and CRMP3−/− (*D*) mice. *E)* Representative tortuous dendrite. *F, G)* Representative alvear axons from WT (*F*) and CRMP3−/− (*G*) mice. White arrow: straight dendrite; Black arrow: tortuous dendrite. Quantitative analysis of apical dentrites: *H*) The numbers of undulating and straight primary dendrites were counted in 8–10 fields for each animal, and results were expressed as undulating dendrites in percentage of the total number of apical primary dendrites per field (0.015 cm^2). The graph represents the average of 1764 and 1605 pyramidal neurons from the WT and CRMP3−/−, respectively. *I)* Dendritic linearity index. The graph represents 52 and 77 measurements with an image analyzer system from the WT and CRMP3−/− mice, respectively. *J)* Camera lucida drawings with 40×lens of 32 neurons/genotype were used to count the number of branching points. The unique apical dendrite extending from the pyramidal cell soma was defined as primary dendrite (PD), dendrites extending from PD as secondary dendrites (SD), and those extending from SD as tertiary dendrites (TD). Higher-order dendrites were not measured. *K)* Average total dendritic length (PD+SD+TD) of 32 neurons/genotype. Neurons from CRMP3−/− showed a significant decrease in dendritic length. Morphometric analysis of basilar dendrites: (*L*) Number of basal somata stem (BSS)/cell expressed as percentage of total cell count (WT 342; CRMP3−/− 315). In CRMP3−/− mice, cell distribution was shifted with more cells having lower number of BSS per cell as compared to WT. **P* <0.01; ***P* <0.05. All statistics for quantitative analysis were performed using average measurement per animal with 4 animals for each genotype.

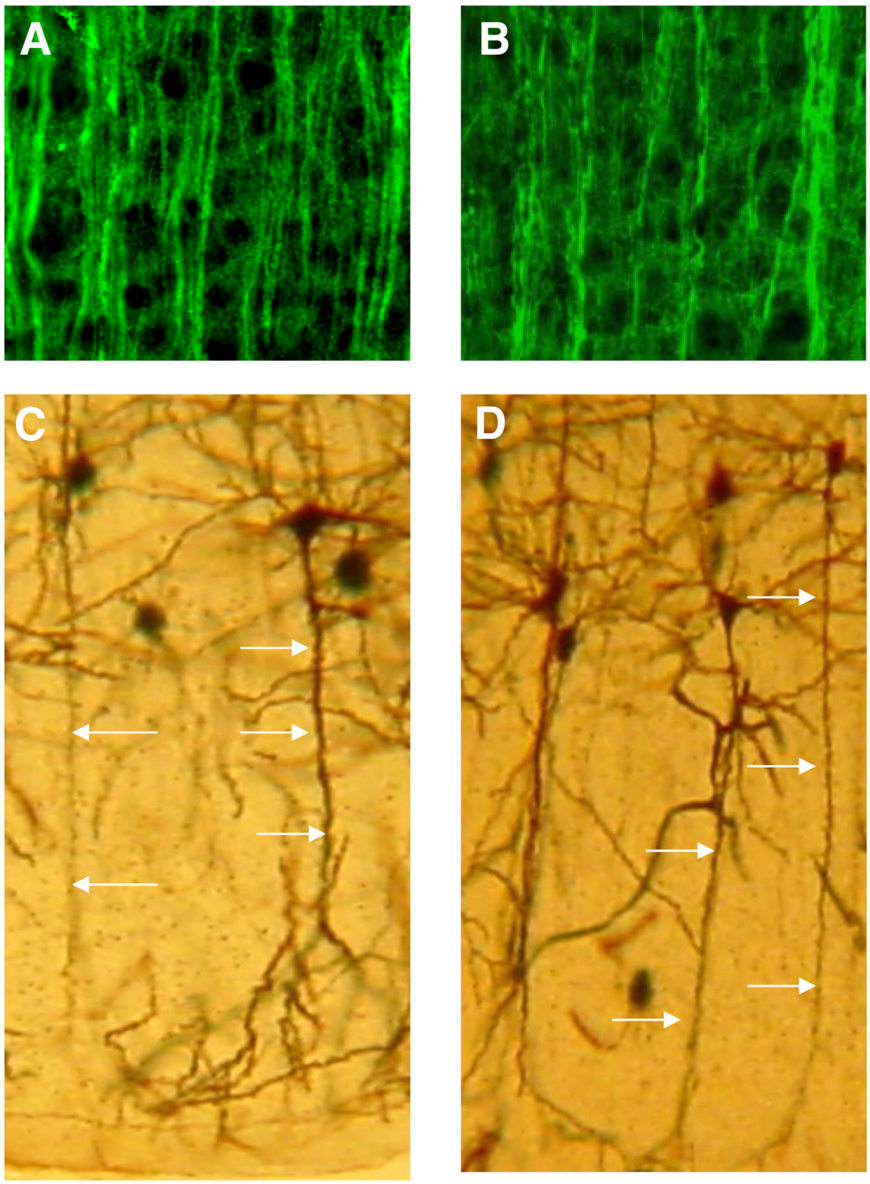

Figure 3.
Normal morphology of cortical neurons. MAP2 (*A–B*) and Golgi (*C–D*) staining of coronal section of cortex of 3 month old WT (*A, C*) and CRMP3−/− (*B, D*) mice. Dendrites from cortical pyramidal neurons from CRMP3−/− mice were not undulated.

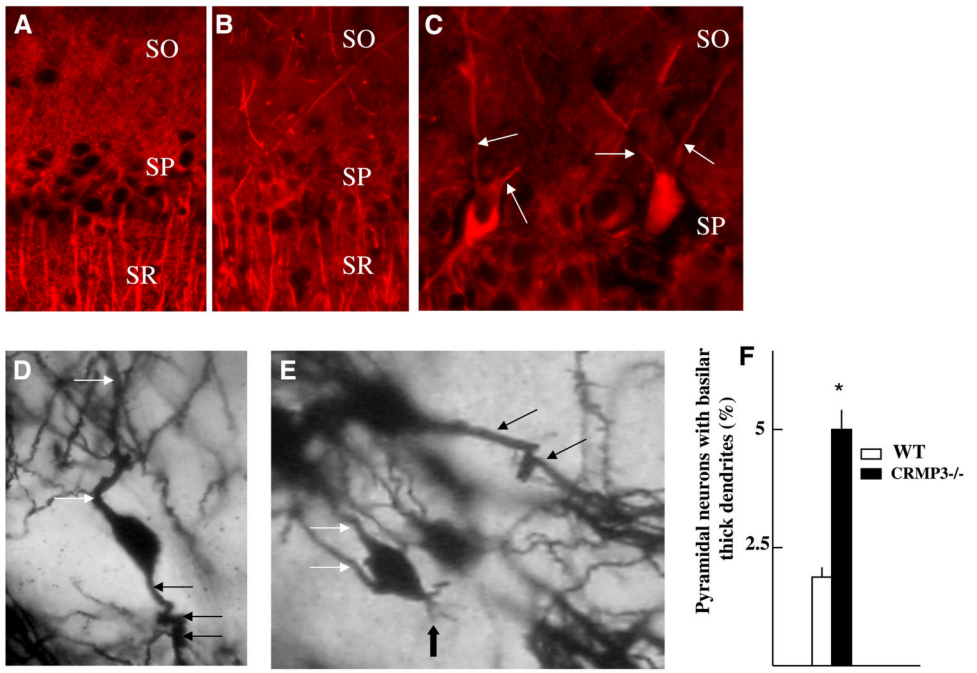

Figure 4.

Presence of thick dendrites in SO. MAP2 (*A–C*) and Golgi (*D–E*) staining show thick neurites extending into SO of CA1 field of CRMP3−/− (*B, C*) but not WT (*A*) mice. *D)* Cells with apical primary dendrite and thick basilar dendrites projecting into SO are present in both genotypes. *E)* Some cells apparently lacked typical single primary apical dendrite and instead exhibited several thin neuritic processes in CRMP3−/− mice. These features were not present in WT mice. Black arrows: apical dendrites; white arrows: thick basilar dendrites; thick black arrow: thin neuritic processes. *F)* Number of cells with thick neurites/field expressed as percentage of total pyramidal cells present in the field (30 fields/genotype; * $P < 0.01$.

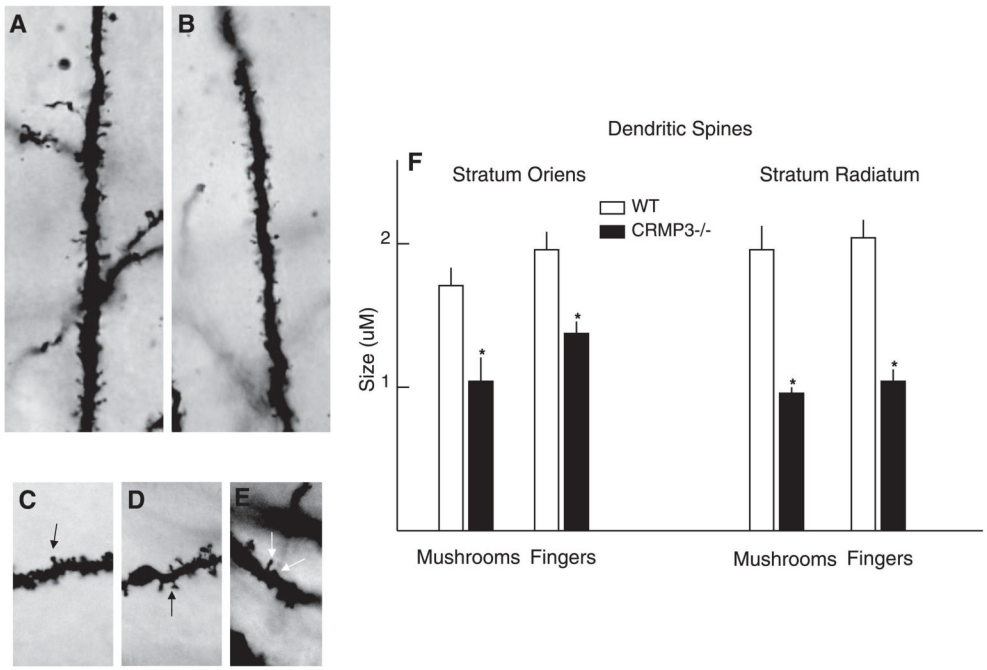

Figure 5.

Dendritic spine alterations in hippocampal pyramidal cells. Representative Golgi-stained dendrite of CA1 pyramidal cells from WT (*A*) and CRMP3−/− (*B*) illustrating the density of individual spines along its length. Note the different types of spines (arrows): mushroom (*C*), cup (*D*), finger (*E*), and stubby (*E*). Quantification of the length of the spines: measurements were made of 2000–2200 spines/genotype (*F*) (**P*<0.003). The lengths of cup and stubby spines are not significantly different between genotypes (see Supplemental Information, T.2)

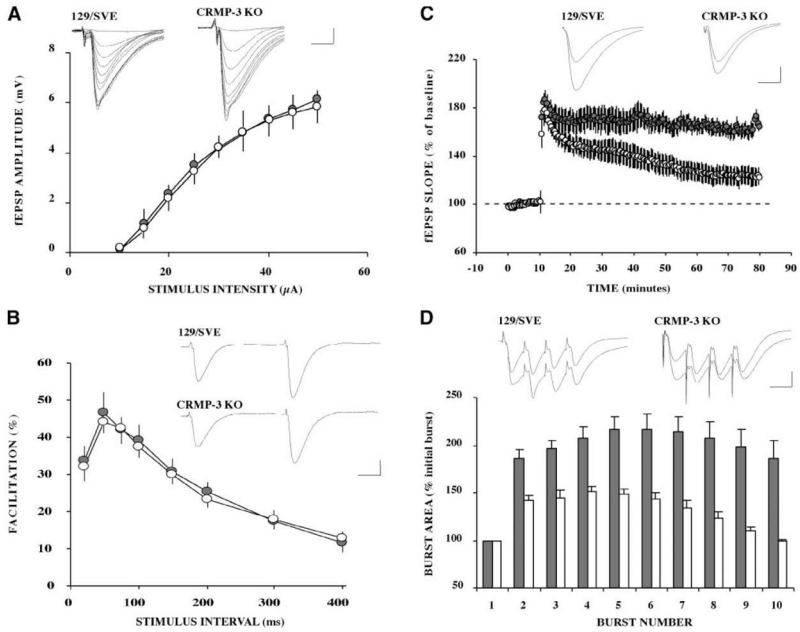

Figure 6.

LTP impairment in hippocampal slices from CRMP3−/− mice. Electrophysiological parameters in hippocampal slices from WT (closed circles and bars) and CRMP3−/− (open circles and bars) mice, *n* =7. *A)* Input-output responses. No significant differences in fEPSP amplitudes were found between WT and CRMP3−/− mice. Insert: representative field responses in WT and CRMP3−/−. Calibration bars: 5 ms, 1 mV. *B)* Paired-pulse facilitation. The degree of paired-pulse facilitation of fEPSP amplitude was expressed as a function of the interpulse interval. Insert: representative field responses. Calibration bars: 10 ms, 1 mV. *C)* LTP formation. TBS was applied and produced stable LTP in WT mice. The same stimulation resulted in an initial potentiation in CRMP3−/− mice that decayed over time. Insert: representative field response 2 min before and 60 min after TBS. Calibration bars: 5 ms, 1 mV. *D)* Burst response. Depolarization elicited in slices from CRMP3−/− mice was significantly less than from WT. Insert: representative recordings of the 4 fEPSPs of a burst response; burst number 1 (top) and 8 (bottom) are superimposed for both animals. Calibration bars: 10 ms, 1 mV.